First-principles study of liquid and amorphous Sb_2Te_3

S. Caravati,[1] M. Bernasconi,[2,*] and M. Parrinello[1]

[1]*Department of Chemistry and Applied Biosciences, ETH Zurich, USI Campus, Via Giuseppe Buffi 13, 6900 Lugano, Switzerland*
[2]*Dipartimento di Scienza dei Materiali and CNISM, Università di Milano-Bicocca, Via R. Cozzi 53, I-20125 Milano, Italy*

Based on *ab initio* molecular-dynamics simulations, we generated models of liquid and amorphous Sb_2Te_3 of interest for applications as phase change material in optical and electronic data storage. The local geometries of Sb and Te atoms in a-Sb_2Te_3 are similar to that found in the extensively studied $Ge_2Sb_2Te_5$ and GeTe phase change materials already exploited for nonvolatile memory applications. Analysis of the vibrational properties and electronic structure of a-Sb_2Te_3 is presented and compared to the crystalline counterparts.

I. INTRODUCTION

Chalcogenide alloys are interesting materials for information storage. Several compounds in this class undergo a fast and reversible crystal-to-amorphous phase change, exploited in optical data storage (digital versatile disk) (Ref. [1]) and electronic phase change memories (PCM).[1–3] While doped SbTe alloys close to the eutectic composition are often used in optical storage media, pseudobinary alloys along the GeTe-Sb_2Te_3 tie line are mostly studied for PCM applications.[1] In particular, the binary compound Sb_2Te_3 shows very high crystallization speed and low reset power because of its relatively low melting point. Although the low crystallization temperature (<100 °C) prevents its practical application in PCM, doping with other elements (with nitrogen the most promising) is under scrutiny to improve the stability of the amorphous phase.[4]

In this paper, we investigate the properties of models of amorphous Sb_2Te_3 (a-Sb_2Te_3) generated by quenching from the melt within first-principles molecular-dynamics simulations. Information on the microscopic properties of a-Sb_2Te_3 are of interest for sake of comparison to the properties of compounds along the pseudobinary $(GeTe)_x$-$(Sb_2Te_3)_y$ line and in particular $(GeTe)_2(Sb_2Te_3)$ (GST), the prototypical phase change material for PCM applications.

In a previous work, we have generated a 270-atom model of amorphous GST by quenching from the melt within first-principles molecular dynamics. In our a-GST model,[5,6] most of Ge and Sb atoms are four-coordinated while Te is mostly three-coordinated in defective octahedral-like sites which recall the local environment of cubic crystalline GST. However, as many as one third of Ge atoms are in a tetrahedral geometry, as proposed by extended x-ray absorption fine structure and x-ray absorption near-edge spectroscopy (EXAFS and XANES) measurements.[7] This configuration is absent in the crystalline phase and favored in a-GST by the presence of homopolar (Ge-Ge and Ge-Sb) bonds.[5] Similar results on the structural properties of a-GST have been obtained from *ab initio* simulations by other groups.[8–10] A question which naturally arises is whether Sb and Te atoms in a-Sb_2Te_3 were in a local geometrical environment (but for the presence of Ge) similar to those found in the ternary GST compound. In this paper, we address this issue along with providing a detailed analysis of the electronic and vibrational

properties of a-Sb_2Te_3. For sake of comparison, information on the structural and electronic properties of the liquid phase close to the melting point are given as well.

II. COMPUTATIONAL DETAILS

The amorphous model was generated by quenching from the melt within *ab initio* molecular-dynamics simulations by using the scheme of Kühne *et al.*[11] In the spirit of the Car-Parrinello (CP) approach, the wave functions are not self-consistently optimized during the dynamics. However, in contrast to CP, large integration time steps can be used in the simulation. This scheme leads to a slightly dissipative dynamics of the type $\gamma_D \dot{\mathbf{R}}_I$, where $\mathbf{R}_I$ are the ionic coordinates. In Ref. [11], it is shown how to compensate for this dissipation and obtain a correct canonical sampling. This scheme is implemented in the CP2K suite of programs.[12,13] We used the generalized gradient approximation (GGA) to the exchange-correlation functional as proposed by Perdew-Burke-
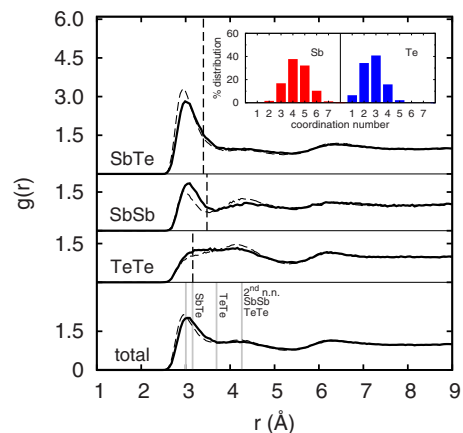

FIG. 1. (Color online) Total and partial pair-correlation functions of l-Sb_2Te_3. Continuous (dashed) lines correspond to the PBE (LDA) functional. The first maximum for PBE data is at position 3.02 Å (Sb-Te) and 3.07 Å (Sb-Sb). (Inset) Distribution of coordination numbers of different species obtained by integration of the partial pair-correlation functions (PBE) up to the bonding cutoff indicated by the vertical lines. Vertical lines on the total correlation function indicate instead the position of the maxima in the partial pair-correlation functions of crystalline Sb_2Te_3 (Refs. [22] and [23]).

TABLE I. Average coordination number for different pairs of atoms computed from the partial pair-correlation functions (PBE data in Fig. 5) for a-Sb$_2$Te$_3$. Data for l-Sb$_2$Te$_3$ are given in parenthesis.

	With Sb	With Te	Total
Sb	0.458 (1.360)	3.635 (3.006)	4.093 (4.367)
Te	2.424 (2.004)	0.319 (0.722)	2.743 (2.727)

Ernzerhof (PBE).[14] Selected calculations were repeated also by using the simple local-density approximation (LDA). Goedecker-type pseudopotentials[15] with five and six valence electrons were adopted for Sb and Te, respectively. The Kohn-Sham (KS) orbitals were expanded in a triple-zeta-valence plus polarization (TZVP) Gaussian-type basis set[16] and the charge density was expanded in a plane-wave basis set with a cutoff of 100 Ry to efficiently solve the Poisson equation within the QUICKSTEP scheme.[12,13] Brillouin-zone integration was restricted to the supercell Γ point. A time step of 2 fs was used for the simulations. The same scheme was applied in our previous work on GST.[5,6] We used a cubic supercell with edge 20.44 Å long (240 atoms) at the density of the liquid phase at 1003 K at normal pressure (0.0281 atoms/Å^3).[17] Atoms were initially arranged in the crystalline trigonal geometry stretched in such a way as to fit into the cubic box. The system was then heated and equilibrated for 15 ps at 2300 K in the liquid phase and then quenched in 2 ps and further equilibrated for 10 ps at 1003 K. The parameter $\gamma_D = 3.6 \times 10^{-4}$ fs^{-1} was determined as in the Ref. 11. In order to generate a model of a-Sb$_2$Te$_3$, the liquid was brought to 300 K in 50 ps.

III. RESULTS

A. Liquid phase

The pair-correlation functions and the distribution of co-ordination numbers of the liquid phase at 1003 K at the experimental density (0.0281 atoms/Å^3) (Ref. 17) are reported in Fig. 1. Average coordination numbers for the different species are given in Table I. A large fraction of ho-
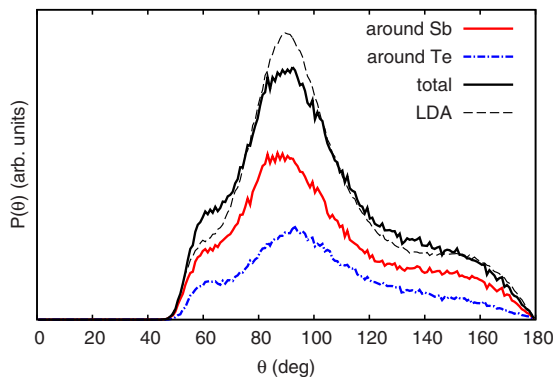

FIG. 2. (Color online) Angle distribution functions of l-Sb$_2$Te$_3$ at the PBE level. The total angle distribution function is reported for LDA functional as well (dashed line).
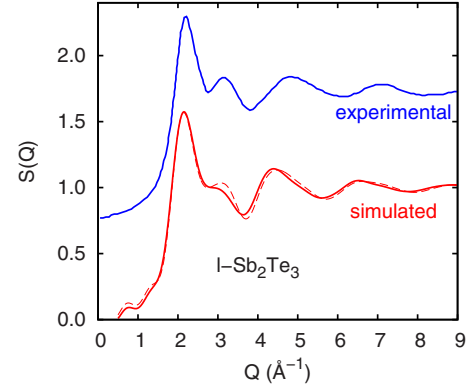

FIG. 3. (Color online) X-ray-weighted (Eq. 56 in Ref. 18 with the Q-dependent x-ray atomic form factors) total scattering function $S(Q)$ of l-Sb$_2$Te$_3$ at 1003 K compared to experimental x-ray data at the same temperature from Ref. 19. The continuous (dashed) theoretical lines correspond to PBE (LDA) results.

mopolar Sb-Sb and Te-Te bonds is present. The angle distribution function is shown in Fig. 2. The broad peaks at $\sim 90°$ and around $\sim 170°$ indicate the presence of an octahedral-like geometry similar to that of the crystalline phase. Both PBE and LDA results are presented. The calculated x-ray and neutron-weighted total scattering functions $S(Q)$ of l-Sb$_2$Te$_3$ are compared to x-ray data in Fig. 3. The small misfit in the positions of the peaks at large Q indicates a systematic overestimation of the bond lengths as already documented for GST.[6] The situation is only marginally improved by using the LDA functional. From the analysis of the structure factor of several chalcogenide liquids, it was proposed[20] that the ratio between the heights of the first two peaks of $S(Q)$ is an indicator of the local bonding geometry. Namely, the quantity $S = S(Q_2)/S(Q_1)$, where Q_1 and Q_2 are the positions of the first two peaks of the structure factor, is greater than 1 for a tetrahedral liquid and smaller than 1 for an octahedral liquid. Our model of l-Sb$_2$Te$_3$ is an octahedral liquid and indeed $S < 1$ which further confirms the correlation proposed in Ref. 20. The liquid is metallic with a high density of states at the Fermi level as shown in Fig. 4.

B. Amorphous phase

Structural properties. The theoretical equilibrium density of the amorphous phase was computed from a Murnaghan
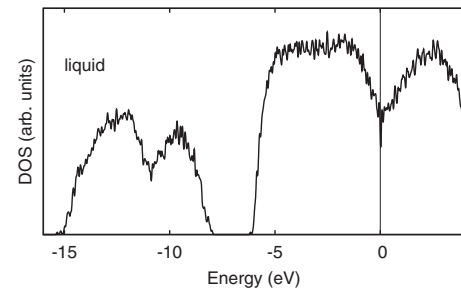

FIG. 4. Electronic density of states of l-Sb$_2$Te$_3$ computed with the HSE03 functional (cf. Sec. III B) and averaged over 15 configurations at 1003 K. The Kohn-Sham energies are broadened with Gaussian functions 27 meV wide. The zero of energy corresponds to the Fermi level.
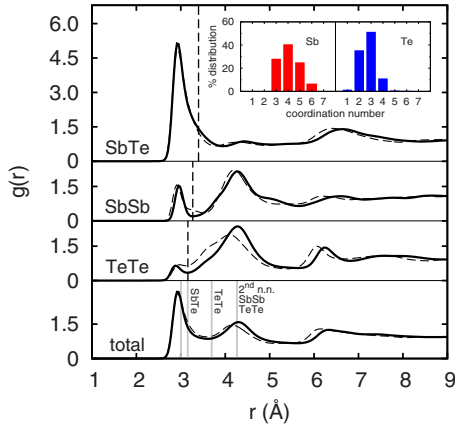
FIG. 5. (Color online) Total and partial pair-correlation functions of a-Sb_2Te_3. Continuous (dashed) lines correspond to the PBE (LDA) functional. The first maximum (PBE data) is at positions 2.93 Å (Sb-Te), 2.97 Å (Sb-Sb), and 2.93 Å (Te-Te). (Inset) Distribution of coordination numbers (PBE) of different species obtained by integration of the partial pair-correlation functions up to the bonding cutoff indicated by the vertical lines. Vertical lines on the total correlation function indicate instead the position of the maxima in the partial pair-correlation functions of crystalline Sb_2Te_3 (Refs. 22 and 23).

fitting of the energy-volume data from the optimized geometries at zero temperature. The theoretical equilibrium density (0.0271 atoms/Å³) turned out to be very similar to that of the liquid at the melting point [0.0281 atoms/Å³ (Ref. 17)]. The calculated bulk modulus and derivative of the bulk modulus with respect to pressure are 11 GPa and 9.3, respectively. Previous calculations on GST (Ref. 6) revealed that simple LDA performs better than GGA functionals in reproducing the bulk modulus of both crystalline and amorphous phases with marginal changes in the structural properties, but for an increase in the equilibrium density (3% and 7% with respect to experiments for c-GST and a-GST, respectively). The LDA calculation of the equation of state of a-Sb_2Te_3 yielded an equilibrium density of 0.0314 atoms/Å³ and a bulk modulus of 27 GPa. The change in the structural properties due the change in the functional from GGA and LDA is similar to that already documented for GST.[6] We are not aware of experimental data on the density of the amorphous
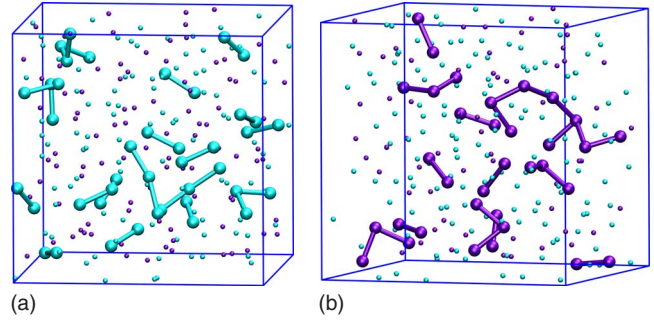

FIG. 6. (Color online) Distribution (PBE) of (a) Te-Te homopolar bonds and (b) Sb-Sb homopolar bonds in a-Sb_2Te_3. Te atoms form dimers, trimers, and a single four-membered chain. Smaller spheres depict Sb and Te atoms without homopolar bonds.

phase. All the results discussed hereafter refer to PBE calculations if not otherwise specified. Selected data in the figures are given for the LDA functional as well as detailed in the captions.

The pair-correlation functions and the distribution of coordination numbers of the amorphous model are reported in Fig. 5. Average coordination numbers for the different species are given in Table I. Similarly to a-GST,[5] Sb atoms are mostly four-coordinated and Te atoms are mostly three-coordinated. Sb form bonds preferentially with Te atoms. We observed a large fraction of homopolar Sb-Sb bonds, although smaller than in the liquid phase, namely, 35% of Sb are bonded with at least another Sb (cf. Fig. 6). The concentration of Te-Te bonds is somehow lower, 28.5% of Te atoms being involved in homopolar Te-Te bonds arranged into dimers and trimers (see Fig. 6) and a short four-membered chain. Long chains of Te are not found in a-Sb_2Te_3 while a slightly longer (six-membered) Sb chain can be noticed. Similar results for the environment of Sb and Te were found for a-GST.[5,6,8,9] The distribution of different environment of Sb and Te in a-Sb_2Te_3 is reported in Table II.

Insight on the local geometry of a-Sb_2Te_3 is gained from the angle distribution function in Fig. 7. The broad peak at $\sim$90° and the weaker structure around $\sim$170° are reminiscent of the octahedral-like geometry of the crystalline phase. Angles at $\sim$90° and $\sim$180° clearly dominate the bonding network. For Te, only angles at $\sim$90° are found. However,

TABLE II. Statistics of Te and Sb coordination environments in a-Sb_2Te_3 (PBE data). The percentages of the total number of atoms of each element are given for configurations with a weight greater than 1%.

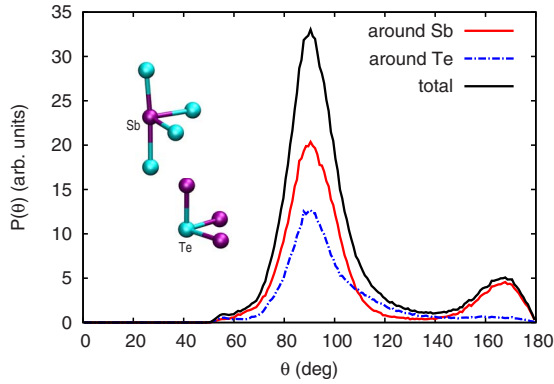|	1	2	3	4	5	6
Sb:			28.1	40.6	25.0	6.3
			Te_3: 15.6	Te_4: 21.9	Te_5: 21.9	Te_6: 5.2
			$SbTe_2$: 7.3	$SbTe_3$: 15.6	$SbTe_4$: 3.1	Sb_2Te_4: 1.1
			Sb_2Te: 4.2	Sb_2Te_2: 3.1		
			Sb_3: 1.0			
Te:	1.4	35.4	51.4	11.1	<1	
	Sb: 1.4	Sb_2: 21.5	Sb_3: 38.2	Sb_3Te: 1.4		
		SbTe: 11.1	Sb_2Te: 12.5	Sb_4: 9.7		
		Te_2: 2.8	$SbTe_2$: <1			

FIG. 7. (Color online) Angle distribution function of a-Sb_2Te_3 with PBE functional. (Inset) Defective octahedral environment for Sb and Te.

the main coordinations of Sb and Te of four and three, respectively, are lower than the ideal octahedral value of six. In our model, and similarly to a-GST,[5,6,8] the presence of neighboring vacancies is responsible for the lower coordination while the bonding angles remain close to $\sim 90°$ and $\sim 180°$ as in the crystalline phase.[22] As occurs in a-GST, Sb and Te are always in the defective octahedral environment depicted in Fig. 7. In a-GST, also the majority of Ge atoms is in a defective octahedral environment mostly with coordination four,[5] but one third of Ge atoms sit in a tetrahedral environment promoted by the presence of Ge-Ge and Ge-Sb bonds.[5] No Sb or Te in tetrahedral sites is observed in a-GST or in Sb_2Te_3. This is demonstrated by looking at the distribution of the order parameter q in Fig. 8. The local order parameter q that we introduced in Ref. 5 is a measure of tetrahedricity of the local environment and it is defined by $q = \frac{1}{3} - \frac{3}{8} \Sigma_{i>k} (\frac{1}{3} + \cos \theta_{ijk})^2$ where the sum runs over the couples of atoms bonded to a central atom j. $q = 1$ for the ideal tetrahedral geometry, $q = 0$ for the six-coordinated octahedral site, and $q = 5/8$ for a four-coordinated defective octahedral site.

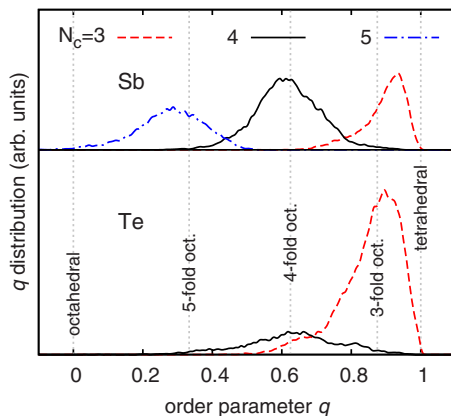Turning now to the medium range order of a-Sb_2Te_3, we report the ring distribution in Fig. 9. As occurs in a-GST, the

FIG. 8. (Color online) Distribution of the local order parameter q (see text) for Sb and Te in a-Sb_2Te_3 (PBE data). Vertical lines indicate the values of q for selected ideal geometries. All Te and Sb atoms are in defective octahedral environments. N_c indicates the coordination number.
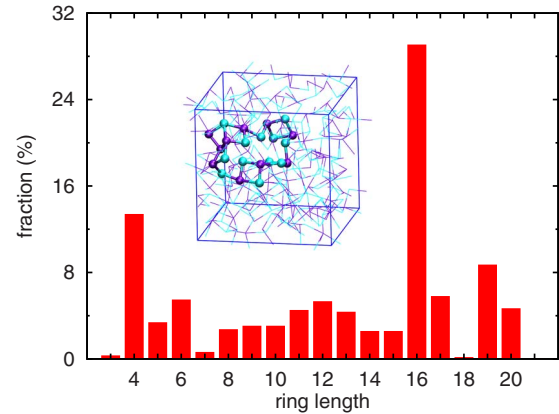

FIG. 9. (Color online) Ring distribution function of a-Sb_2Te_3 computed as in Ref. 24 (PBE data). (Inset) Snapshot of a large 16-membered ring formed by a sort of belt made by short rings.

four-membered ring is the most abundant among the smaller ones. A large fraction of four-membered rings (85.5%) is made by $ABAB$ rings (A=Sb and B=Te) typical of the crystalline phase without homopolar bonds. One notes a large percentage of very large 16-membered rings. A snapshot of one of those is shown in the inset of Fig. 9. Actually, the large ring is a sort of belt made of smaller rings. Therefore several 16-membered rings counted in the statistics correspond to rings running along a single belt structure. These features indicate that a-Sb_2Te_3 is a structure more open than that of the ternary GST.

Based on the structural analysis of *ab initio* models of amorphous GST and GeTe, Akola and Jones[8] proposed that the presence of cavities favors a rapid reorientation of the four-membered rings speeding up the crystallization process. Indeed a larger concentration of cavities is found in a-GST than in a-GeTe, in agreement with the higher experimental crystallization temperature of the latter. To quantify the concentration of these cavities (or voids) in a-Sb_2Te_3, we have followed a procedure similar to that introduced by Akola and Jones.[8] First, cavity domains are defined as the free space outside spheres centered on each atom with a radius corresponding to 90% of the average bond length for each species. For instance, the average bond length for Sb is obtained by weighting the maximum of the Sb-Sb and Sb-Te pair-correlation functions by the corresponding pair coordination number. Inside each disconnected cavity domain, we then identify cavity centers as the points which are maximally distant from all neighboring atoms. In the presence of very elongated cavity, more than one point might fit into this region (by excluding points which are too close each other, e.g., closer than 1 Å). Then, we construct Voronoi polyhedra around the cavity centers by considering bonds formed among centers inside the same cavity and among such centers and atoms. Finally the volume of the cavity is obtained as the volume of the connected Voronoi polyhedra around the centers inside the cavity itself. It turns out that the volume occupied by cavities is as large as 28% of the total volume in amorphous Sb_2Te_3. We repeated this analysis for the model of a-GST (270 atoms) discussed in Ref. 6 and for a model of amorphous GeTe (216 atoms) quenched from the melt (1220
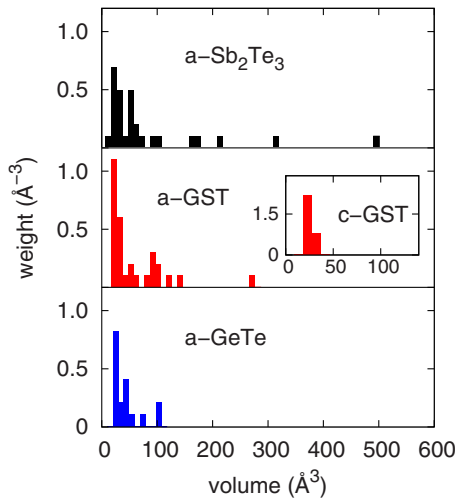
FIG. 10. (Color online) Distribution of the volume of cavities (PBE data) in a-Sb_2Te_3 (theoretical equilibrium density), a-GST, and a-GeTe (exp. equilibrium densities) computed according to Ref. 27. (Inset) The distribution for c-GST at the experimental equilibrium density.

K) in 60 ps,[21] both at the experimental density of the amorphous phases. The volume occupied by cavities is 20% of the total volume in a-GST (10% in cubic crystalline GST as it should) and 14% in a-GeTe.

We also employed a different procedure for the definition of the cavities as proposed in Ref. 27. This procedure is based on a generalized Voronoi-Delaunay analysis which accounts for multicomponent systems that can be regarded as ensembles of atoms of different radii. In a polydisperse system, atomic volumes are delimited by the "Voronoi S surfaces" (VS surfaces), defined as the geometric locus of points equidistant from the surfaces of two atomic spheres instead of their centers. VS surfaces are no more planes as for Voronoi polyhedra but hyperboloids and their intersection gives rise to curved edges (VS channels) and vertexes (VS vertexes). An interstitial sphere with radius R_i, tangent to neighbor atoms, is associated with each VS vertex while each VS channel is characterized by a bottleneck radius R_b which determines the maximum size of a test particle moving along this channel. The network of VS vertexes and VS channels can be used to distinguish interatomic voids and resolve connected cavities, in fact, a natural way of defining voids is through the value of the radius (R_P) of a probe (test sphere) that can be put in the given void. Thus, voids are the parts of the interatomic space that are accessible for a given probe ($R_i \geq R_P$, R_i criterion). On the other hand, if a probe can move along an S-network bond (i.e., pass through a bottleneck) then both VS vertexes connected by this bond belong to the same cavity (R_b criterion). To compute the volume of voids, the VS network is built again taking into account also VS vertexes identified through the R_i criterion as new particles with radius R_i. The volume of each void is calculated numerically through a local mesh, dense enough to minimize the error below a threshold (here: 1.5×10^{-4} Å^3). We applied this analysis by choosing atomic radii as 50% of the average bond length for each species (atomic spheres are partially overlapping or tangent along
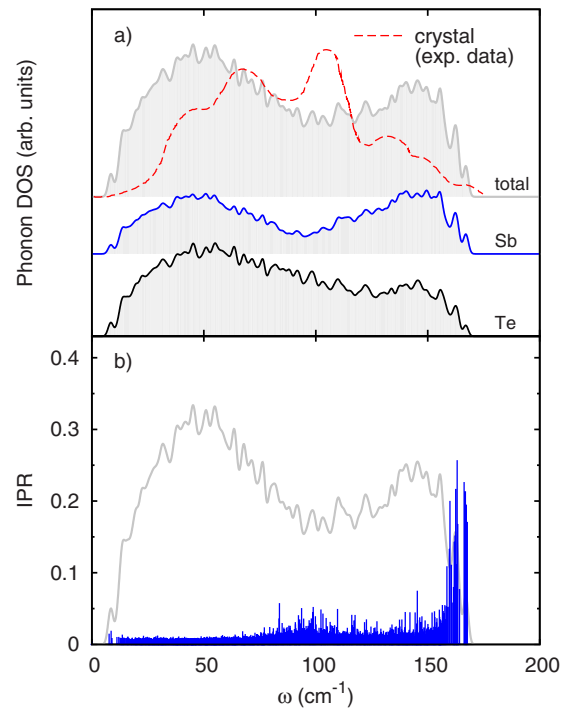

FIG. 11. (Color online) (a) Theoretical phonon DOS of a-Sb_2Te_3 compared to the experimental DOS of the crystalline phase measured from inelastic neutron scattering (Ref. 25). Projections of the phonon DOS of a-Sb_2Te_3 on different species (Te, Sb) are also reported. (b) IPR for phonons in a-Sb_2Te_3 (blue spikes, left scale, see text for definition) superimposed to the density of states.

bonds) and we obtain the VS network through the algorithm presented in Ref. 28, as implemented in the VNP program.[29] By setting the parameter R_P to 1.3 Å, we obtained a total cavity volumes of 27%, 19%, and 12% for a-Sb_2Te_3, a-GST, and a-GeTe, respectively, which are very close to the values given previously. The distribution of the volume of the cavities is compared in Fig. 10 for a-Sb_2Te_3, a-GST, and a-GeTe as computed with the method of Ref. 27. The cavities are in larger number and larger in size in a-Sb_2Te_3 than in the other two compounds. However, we have compared so far results obtained at the experimental equilibrium density for a-GST and a-GeTe and at the theoretical equilibrium density for a-Sb_2Te_3. The larger concentration of cavities in a-Sb_2Te_3 might partially results from an underestimation of the equilibrium density by the PBE functional. In fact, the total volume of the cavities in a-GST and a-GeTe raises to 27% and 21% when computed at the theoretical equilibrium volume of the amorphous phases (5% and 7% larger than in experiments, respectively). We cannot exclude, however, that the PBE error in the equilibrium density might be larger in a-GST and a-GeTe than in a-Sb_2Te_3 for which, unfortunately, the equilibrium experimental density is not known. As already mentioned, Akola and Jones[8] proposed that the presence of nanocavities favors the crystallization. On the other hand, we might also envisage that tetrahedral sites which are not present in the crystalline phases would hinder crystallization. The concentration of tetrahedral sites (associated to Ge only) is zero in Sb_2Te_3, intermediate in a-GST (7% of the total number of atoms), and the highest in a-GeTe (12% of
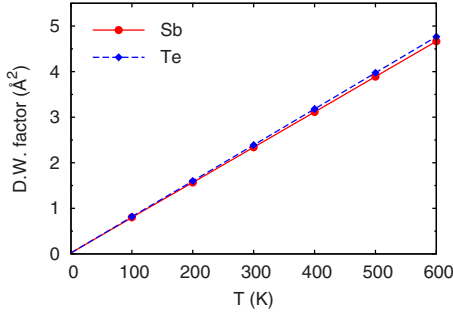
FIG. 12. (Color online) Debye-Waller factor B_κ (see text) of Te and Sb atoms for a-Sb_2Te_3 as a function of temperature.

the total number of atoms).[6,21] Both the concentrations of cavities and the tetrahedral sites correlate indeed with the crystallization temperature which is the lowest in Sb_2Te_3, intermediate in a-GST, and the highest in GeTe.[30,31] However, the crystallization temperature is also more simply correlated with the melting temperature which gives a measure of the bonding strength (higher for Ge-Te than for Sb-Te). For these systems, the crystallization temperature T_c is often defined as the temperature at which one observes a sudden drop in the resistivity by increasing temperature at a constant rate. From the analysis of the resistivity as a function of time, one can also measure the time needed to complete the transformation at T_c (which depends on the material). The so-defined crystallization speed at T_c actually does not correlate with the concentration of cavities or of tetrahedral sites. In fact, the crystallization speed at T_c of a-GST is actually lower than that a-GeTe, although a-GST has a higher concentration of cavities and less tetrahedral sites along with a lower T_c than a-GeTe. We remark that a-GST and a-GeTe display the same type of nucleation dominant crystallization behavior (crystallization controlled by the proliferation of nuclei which grow slowly). The role of the network topology in controlling the crystallization speed thus deserves further investigation.

Vibrational properties. Turning now to the vibrational properties, we computed the phonon frequencies of a-Sb_2Te_3 by diagonalizing the dynamical matrix obtained in turn from the variation of atomic forces due to finite atomic displacements 0.0053 Å large. Only phonons with the periodicity of our supercell (Γ point phonons) were considered. In a previous work, we have already shown that the density functional theory (DFT)-PBE framework is able to reproduce very well the vibrational properties, including Raman and infrared spectra, of crystalline Sb_2Te_3.[23] The phonon density of states of a-Sb_2Te_3 are compared in Fig. 11 to the experimental density of states (DOS) for the crystalline phase as measured by inelastic neutron scattering.[25] Phonon DOSs projected on the different species (Te, Sb) are also shown. In an amorphous material, phonons display localization properties which depend on frequency. To address this issue, we have computed the inverse participation ratio (IPR) of the jth vibrational mode defined as
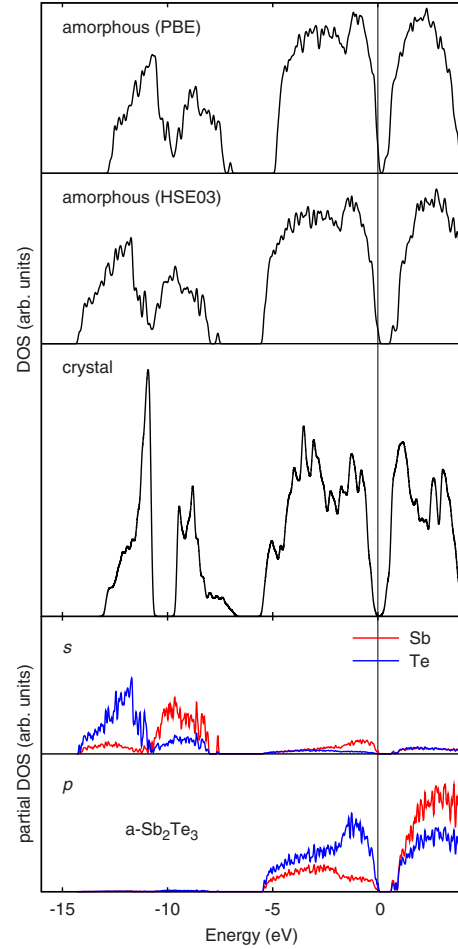

FIG. 13. (Color online) Electronic density of states of amorphous and crystalline Sb_2Te_3 (from Ref. 23). The DOS of the amorphous phase is computed both with the PBE and HSE03 functionals. Projections of the HSE03 DOS of a-Sb_2Te_3 on atomic s and p pseudowave functions are also given. The contribution from d pseudowave functions is negligible on the scale of the figure and it is omitted. The zero of energy corresponds to the highest occupied molecular orbital (top of the valence band). The Kohn-Sham energies of a-Sb_2Te_3 are broadened with Gaussian functions 27 meV wide (responsible for the small DOS above 0 eV).

$$\text{IPR} = \frac{\sum_\kappa \left| \frac{\mathbf{e}(j,\kappa)}{\sqrt{M_\kappa}} \right|^4}{\left(\sum_\kappa \frac{|\mathbf{e}(j,\kappa)|^2}{M_\kappa} \right)^2}, \qquad (1)$$

where $\mathbf{e}(j,\kappa)$ are phonon eigenvectors and the sum over κ runs over the N atoms in the unit cell with masses M_κ. According to this definition, the value of IPR varies from $1/N$ for a completely delocalized phonon to one for a mode completely localized on a single atom. The values of IPR for a-Sb_2Te_3 are reported in Fig. 11.

The modes above 160 cm^{-1} are strongly localized, each mainly on a bond (Sb-Te or Sb-Sb) connecting atoms with low coordination (Te two-coordinated and Sb three-coordinated) and with length in the shorter tail of the corre-
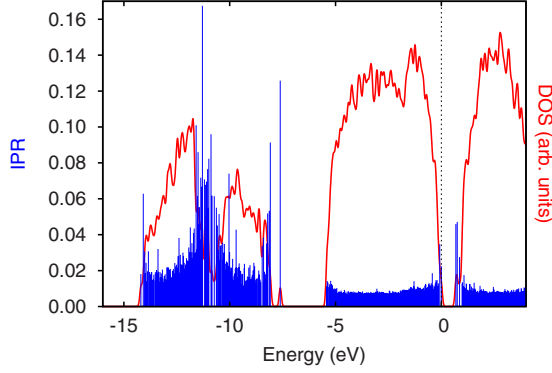
FIG. 14. (Color online) Electronic density of states of a-Sb_2Te_3 (HSE03 functional) and the corresponding values of the (IPR) (blue spikes, left scale, see text for definition). The Kohn-Sham energies are broadened with Gaussian functions 27 meV wide. The zero of energy corresponds to the highest occupied molecular orbital (top of the valence band).

sponding pair-correlation function. From the projected DOS we also computed the Debye-Waller factor for each species defined by[26]

$$B_\kappa = \frac{8\pi^2}{3}\langle \mathbf{u}_\kappa^2 \rangle,$$

where κ runs over the three species and $\langle \mathbf{u}_\kappa^2 \rangle$ is the mean average square displacement of atoms of species κ computed from harmonic phonons as

$$\langle \mathbf{u}_\kappa^2 \rangle = \sum_{j,m} \frac{\hbar}{\omega_j} \frac{|\mathbf{e}(j,m)|^2}{M_\kappa} \left[n_B\left(\frac{\hbar\omega_j}{k_B T}\right) + \frac{1}{2} \right], \qquad (2)$$

where m runs over atoms of species κ, and ω_j and $\mathbf{e}(j,m)$ are frequency and eigenvector of the jth harmonic phonon. The temperature dependence is introduced by the Bose factor $n_B(\frac{\hbar\omega_j}{k_B T})$.

The resulting Debye-Waller factors as a function of temperature, reported in Fig. 12, are similar to those we have previously computed in a-GST.[6] The phonon density of states and Debye-Waller factors computed at the LDA level are given as additional material.[32]

Electronic properties. Electronic DOS of a-Sb_2Te_3 is computed from Kohn-Sham orbitals at the supercell Γ point broadened with a Gaussian function with variance of 27 meV. The electronic DOS of a-Sb_2Te_3 is computed by making use of both the PBE functional and the HSE03 hybrid functional[33] which better reproduces band gaps. The electronic DOS of a-Sb_2Te_3 is compared in Fig. 13 to the crystalline counterpart from Ref. 23 (calculated with PBE functional on a $20 \times 20 \times 20$ mesh in the irreducible Brillouin zone). For the electronic structure of a-Sb_2Te_3, we still used the geometry optimized at the DFT-PBE level of theory. Projection of the DOS on atomic orbitals is also given in Fig. 13 for a-Sb_2Te_3. While l-Sb_2Te_3 is metallic (cf. Fig. 4), our a-Sb_2Te_3 model is semiconducting with a gap 0.69 eV large, in reasonable agreement with the Tauc band gap of 0.5 eV measured by Park *et al.*[34] To quantify the localization properties of individual KS states, we have computed the IPR
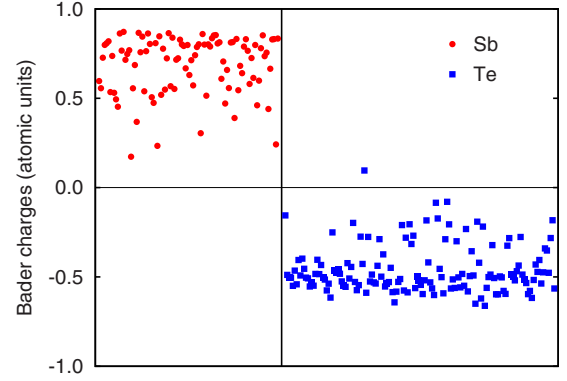

FIG. 15. (Color online) Bader ionic charges (atomic units) of the model of a-Sb_2Te_3. Each point corresponds to an individual atom in the 240-atom supercell.

which is defined for the ith KS state by $\sum_j c_{ij}^4 / (\sum_j c_{ij}^2)^2$, where j runs over the Gaussian-type orbitals (GTOs) of the basis set and c_{ij} are the expansion coefficients of the ith KS state in GTOs. IPRs are given in Fig. 14. Few states at the conduction and valence-band edges are strongly localized due to disorder. However, more strongly localized states are also present deeper in energy.

To identify the possible presence of charged defects, we computed the Bader ionic charges from the total electronic charge density by using the scheme of Ref. 35 (cf. Fig. 15). No highly charged defects such as valence alternation pair (VAP) states[36] are found similarly to what occurs in our models of a-GST (Refs. 5 and 6) and a-GeTe (Ref. 21) possibly due to the lack of long Te chains. Mulliken and Lödin charges are given as additional materials[32] for sake of comparison.

IV. CONCLUSIONS

We have provided a model of liquid Sb_2Te_3 and of the amorphous phase by quenching from the melt within *ab initio* molecular-dynamics simulations similarly to what previously reported for other phase change materials such as $Ge_2Sb_2Te_5$,[5,6,8-10] GeTe,[8,21] and $GeSb_2Te_4$.[37] It turns out that Sb and Te atoms are mostly fourfold and threefold coordinated, respectively, in a defective octahedral sites as occurs in $Ge_2Sb_2Te_5$ (Refs. 5, 6, and 8–10) and $GeSb_2Te_4$.[37] No tetrahedral sites are found in a-Sb_2Te_3 due to the lack of Ge atoms which in a sizable fraction sit in a tetrahedral environment in GST, GeTe, and $GeSb_2Te_4$.[5,6,8,9,37] A large amount of nanocavities is present in the amorphous network of Sb_2Te_3 occupying 28% of the total volume. As occurs in a-GST and a-GeTe, homopolar Te-Te bonds are present in a-Sb_2Te_3 (along with Sb-Sb bonds) in the form of dimers and very small chains (at most four-membered). The lack of long Te chains is probably also at the origin of the lack of VAP defects in a-Sb_2Te_3 which are instead often proposed as typical topological defects in other amorphous chalcogenides.

ACKNOWLEDGMENTS

*marco.bernasconi@mater.unimib.it

[1] M. Wuttig and N. Yamada, Nature Mater. **6**, 824 (2007).

[2] A. L. Lacaita and D. J. Wouters, Phys. Status Solidi A **205**, 2281 (2008).

[3] A. Pirovano, A. L. Lacaita, A. Benvenuti, F. Pellizzer, and R. Bez, IEEE Trans. Electron Devices **51**, 452 (2004).

[4] Y. Yin, H. Sone, and S. Hosaka, J. Appl. Phys. **102**, 064503 (2007).

[5] S. Caravati, M. Bernasconi, T. D. Kühne, M. Krack, and M. Parrinello, Appl. Phys. Lett. **91**, 171906 (2007).

[6] S. Caravati, M. Bernasconi, T. D. Kühne, M. Krack, and M. Parrinello, J. Phys.: Condens. Matter **21**, 255501 (2009).

[7] A. V. Kolobov, P. Fons, A. I. Frenkel, A. L. Ankudinov, J. Tominaga, and T. Uruga, Nature Mater. **3**, 703 (2004).

[8] J. Akola and R. O. Jones, Phys. Rev. B **76**, 235201 (2007).

[9] J. Akola and R. O. Jones, J. Phys.: Condens. Matter **20**, 465103 (2008).

[10] J. Hegedus and S. R. Elliott, Nature Mater. **7**, 399 (2008).

[11] T. D. Kühne, M. Krack, F. R. Mohamed, and M. Parrinello, Phys. Rev. Lett. **98**, 066401 (2007).

[12] M. Krack and M. Parrinello, in *High Performance Computing in Chemistry*, edited by J. Grotendorst, NIC Vol. 25 (NIC-Directors, Jülich, 2004), pp. 29–51; http://cp2k.berlios.de

[13] J. VandeVondele, M. Krack, F. Mohamed, M. Parrinello, T. Chassaing, and J. Hutter, Comput. Phys. Commun. **167**, 103 (2005).

[14] J. P. Perdew, K. Burke, and M. Ernzerhof, Phys. Rev. Lett. **77**, 3865 (1996).

[15] S. Goedecker, M. Teter, and J. Hutter, Phys. Rev. B **54**, 1703 (1996); M. Krack, Theor. Chem. Acc. **114**, 145 (2005).

[16] Extension of the basis set to QZV2P does not introduce sizable change in the pair-correlation functions of GST (Ref. 6).

[17] K. J. Singh, R. Satoh, and Y. Tsuchiya, J. Phys. Soc. Jpn. **72**, 2546 (2003).

[18] D. A. Keen, J. Appl. Crystallogr. **34**, 172 (2001).

[19] T. Satow, O. Uemura, and Y. Sagara, Phys. Status Solidi A **71**, 555 (1982).

[20] C. Steimer, V. Coulet, W. Welnic, H. Dieker, R. Detemple, C. Bichara, B. Beuneu, J.-P. Gaspard, and M. Wuttig, Adv. Mater. **20**, 4535 (2008).

[21] R. Mazzarello, S. Caravati, S. Angioletti-Uberti, M. Bernasconi, and M. Parrinello (unpublished).

[22] T. L. Anderson and H. B. Krause, Acta Crystallogr., Sect. B **30**, 1307 (1974).

[23] G. C. Sosso, S. Caravati, and M. Bernasconi, J. Phys.: Condens. Matter **21**, 095410 (2009).

[24] D. S. Franzblau, Phys. Rev. B **44**, 4925 (1991).

[25] H. Rauh, R. Geick, H. Kohler, N. Nucker, and N. Lehner, J. Phys. C **14**, 2705 (1981).

[26] L.-M. Peng, S. L. Dudarev, and M. J. Whelan, *High Energy Electron Diffraction and Microscopy* (Oxford University Press, Oxford, 2004).

[27] M. G. Alinchenko, A. V. Anikeenko, N. N. Medvedev, V. P. Voloshin, M. Mezei, and P. Jedlovszky, J. Phys. Chem. B **108**, 19056 (2004).

[28] N. N. Medvedev, V. P. Voloshin, V. A. Luchnikov, and M. L. Gavrilova, J. Comput. Chem. **27**, 1676 (2006).

[29] http://www.kinetics.nsc.ru/sms/?Software:VNP

[30] S. Raoux, B. Munoz, H.-Yu. Cheng, and J. L. Jordan-Sweet, Appl. Phys. Lett. **95**, 143118 (2009).

[31] S. Raoux, Annu. Rev. Mater. Res. **39**, 25 (2009).

[32] See supplementary material at http://link.aps.org/supplemental/10.1103/PhysRevB.81.014201 for the phonon density of states and Debye-Waller factor at the LDA level of theory and Mulliken and Löwdin charges of a-Sb_2Te_3.

[33] J. Heyd, G. E. Scuseria, and M. Ernzerhof, J. Chem. Phys. **118**, 8207 (2003).

[34] J.-W. Park *et al.*, Appl. Phys. Lett. **93**, 021914 (2008).

[35] G. Henkelman, A. Arnaldsson, and H. Jonsson, Comput. Mater. Sci. **36**, 354 (2006).

[36] K. Kastner, D. Adler, and H. Fritzshe, Phys. Rev. Lett. **37**, 1504 (1976).

[37] Z. Sun, J. Zhou, A. Blomqvist, B. Johansson, and R. Ahuja, Appl. Phys. Lett. **93**, 061913 (2008).